Agricultural and Forest Meteorology 169 (2013) 195–210

Contents lists available at SciVerse ScienceDirect

Agricultural and Forest Meteorology

journal homepage: www.elsevier.com/locate/agrformet

Turbulence spectra measured during fire front passage

Daisuke Seto[a], Craig B. Clements[a,*], Warren E. Heilman[b]

[a] Department of Meteorology and Climate Science, San José State University, San José, CA 95192, USA
[b] USDA Forest Service, Northern Research Station, East Lansing, MI 48823, USA

ARTICLE INFO

Article history:
Received 20 March 2012
Received in revised form 9 August 2012
Accepted 24 September 2012

Keywords:
Wildland fire
Turbulence
Spectra
Fire–atmosphere interactions

ABSTRACT

Four field experiments were conducted over various fuel and terrain to investigate turbulence generation during the passage of wildland fire fronts. Our results indicate an increase in horizontal mean winds and friction velocity, horizontal and vertical velocity variances as well as a decreased degree of anisotropy in TKE during fire front passage (FFP) due to fire-induced winds. Vertical velocity and temperature variances observed during FFP approached the local free convection prediction when represented as a function of stability parameter z/L under very unstable conditions. The results of our wavelet spectral analysis show increased energy in velocity and temperature spectra at high frequency during FFP for all four cases; we hypothesize this is caused by the shedding of small eddies generated from the fire front. Additionally, spectral energy of velocity components at low frequencies may be affected by cross-flow intensity, topography, presence of canopy layer, and degree of fire–atmosphere coupling. When the velocity spectra are normalized using the friction velocity u_* following Monin–Obukhov scaling, the velocity spectra observed during the FFP collapsed into a fairly narrow band in the inertial subrange, suggesting that as far as inertial range is concerned, the friction velocity u_* is a valid scaling parameter that can be used for wildfire application. When the temperature spectra are normalized by T_*, the temperature spectra observed during the FFP did not show any systematic behaviors predicted by the similarity scaling due to the extreme surface heating environment of fires.

1. Introduction

Recent advances in numerical modeling of fire–atmosphere processes make it possible to simulate both the small-scale fire–atmosphere interactions that occur at spatial scales on the order of tens of meters at the fire front and larger-scale atmospheric forcings affecting the entire fire area that occur at spatial scales on the order of kilometers (Jenkins et al., 2001). However, few, if any, studies have focused on the observed turbulence structure in the immediate environment of propagating fires to further understand the scales of the interaction and therefore, few principles exist from which to describe the behavior of strongly perturbed flow near the surface around the fire front. This is because conducting meteorological measurements near the fire front, even during prescribed fires, is challenging due to the risk of damaging the instrumentation. Consequently, detailed in situ turbulence measurements have been very limited.

In situ turbulence measurements made recently over flat terrain with grass fuels during the FireFlux experiment (Clements et al., 2007, 2008) showed increases in both horizontal and vertical velocity variances at the fire front, with the largest increase in the vertical velocity variance caused by convective motion from large heat flux. The turbulence spectral analysis of the vertical wind velocity, w, measured by Clements et al. (2008) revealed a general increase in the w spectral density at lower frequencies during the fire while the overall shape of the spectral density did not change in the high frequency range. The result suggests that large eddies induced by the fire may contribute to the overall turbulence generation. While the spectral analysis performed by Clements et al. (2008) provides useful information regarding spectral energy modified by a grass fire as reference spectra, more field observations of in situ turbulence data during fires are required for further comparisons. In addition, the spectral analysis of horizontal velocity components is necessary to fully understand the interaction of the fire with the atmosphere.

The ability to predict the rate of fire spread is one of the most important requirements for successful fire suppression, and operational fire spread rate predictions may be improved by accounting for the effect of turbulence and eddies in the ambient wind on fire spread (Sun et al., 2009). Albini (1982, 1983) attempted to combine an empirical representation for the power spectral density of horizontal wind near the ground with a theoretical model in order to predict the variability of fire spread rate and intensity of wind-aided free-burning line fires. His results suggest that free-burning line

* Corresponding author. Tel.: +1 408 924 5275; fax: +1 408 924 5191.
E-mail address: craig.clements@sjsu.edu (C.B. Clements).

0168-1923/$ – see front matter © 2012 Elsevier B.V. All rights reserved.
http://dx.doi.org/10.1016/j.agrformet.2012.09.015

fires are responsive to wind speed variations in the frequency range below 0.1 Hz and fire intensity variations are likely to be nearly periodic at the very low frequency. Furthermore, he found the fire spread rate variability to be rather erratic, with standard deviations exceeding the mean value in many cases for timescales on the order of a minute. It should be noted, however, that power spectra of the fire spread rate and intensity in his study were derived from the wind speed at near mid-flame height in the absence of a fire on the site and therefore, the fire–atmosphere coupling or interaction was not included. Anderson et al. (1982) showed that slight changes in the wind speed observed both upwind from the ignition point and across the path of the fire produced substantial variations in the rate of spread of a head fire. The impact of fire-induced turbulence on the rate of spread variation could not be ruled out for the variations. Wind effects on the geometric and thermal properties of the flame front have been investigated at the field scale by Morandini et al. (2006). Their results suggest that the flame shape, temperature, and heat flux were affected by the observed large-scale wind fluctuations and therefore, they highlighted that the large-scale turbulence plays a significant role on fire spread. While their results provided useful information on the influence of wind on fire, more experiments under a wide range of wind conditions are essential to be more conclusive about the interaction between fire and turbulence.

The characteristics of the atmospheric surface layer (ASL) turbulence spectra have been studied extensively to explore whether data from different sites and heights with different stability conditions display a universal behavior in terms of Monin–Obukhov similarity theory (MOST; see Foken, 2006 for review) (Cava et al., 2001). Spectral analysis of the atmospheric turbulence, by decomposing a series of measurements into frequency components, allows for the general description of turbulence structure in terms of a few scaling parameters as power spectral density reveals how much of the variance is associated with a particular frequency. Within the framework of MOST, Kaimal et al. (1972) demonstrated that all spectra reduce to a family of curves so that they converge into a single set of universal curves in the inertial subrange with a $-5/3$ slope signature but diverge at lower frequencies according to the stability parameter z/L, where z is the measurement height and L the Obukhov length. While the systematic behavior of the velocity and temperature spectra found by Kaimal et al. (1972) supports MOST in terms of the behavior of inertial subrange and thus referred to as an 'ideal' reference for flat terrain, a number of recent studies have identified features that deviate from those predicted by MOST. For example, large scale turbulence is known to contribute the failure of MOST for observed turbulence structure (Katul and Chu, 1998; McNaughton and Laubach, 2000; Zhang et al., 2010). Intermittency may also lead to departure from the theoretical scaling (Kuznetsov et al., 1992; Katul et al., 1994).

The spectral characteristics of turbulence were investigated further to test the validity of the similarity theory under non-ideal conditions. In complex terrain, turbulence characteristics depend strongly upon changes in upwind surface roughness and therefore, it is difficult to draw firm conclusions about turbulence behavior modified by topography. Andreas (1987) showed that increased horizontal spectral energy at lower frequency is due to an effect of topography, and similar modification was also observed in the results by Al-Jiboori et al. (2001). Vertical velocity spectra were observed to be less affected by the effect of topography and thus display very similar spectral properties as those over homogeneous terrain (e.g. Panofsky et al., 1982; Al-Jiboori et al., 2001; Cava et al., 2001). It should be noted that studies of turbulence spectra in complex terrain were focused primarily on hills and changing surface properties rather than in mountain valleys.

Characteristics of turbulence spectra within different plant canopies have been studied extensively, and canopy spectra were summarized in Finnigan (2000). Liu et al. (2001) demonstrated that the maximum turbulent energy of the velocity and temperature inside the forest canopy shift toward higher frequencies as compared with previously observed spectra over flat terrain, emphasizing more contributions from smaller eddies. Their results also indicate that the normalized velocity and temperature spectra obey the $-5/3$ slope in the inertial subrange reasonably well, while Kaimal and Finnigan (1994) suggest a slightly steeper roll-off rate in the inertial subrange for the velocity spectra within the canopy.

The results of the spectral analysis for atmospheric motions have been used for parameterizing eddy diffusivities for air pollution applications (Yadav et al., 1996). For example, the eddy diffusivity coefficients can be specified by using the spectral maximum frequency. The turbulent dissipation rate, estimated from the inertial subrange of the spectra, could also be used for plume rise calculations (Yadav et al., 1996). Additionally, CALPUFF (Scire et al., 2000), a default dispersion model used in BlueSky smoke modeling framework (Larkin et al., 2009) for addressing local and regional smoke impacts caused by wildland fire, includes an option to estimate the dispersion coefficients σ_v and σ_z based on similarity theory. The validity of the similarity theory, however, must be questioned when used for wildland fire applications because the perturbed boundary layer over an extremely heated surface as fire propagates is not well understood in the micrometeorological sense. One of the reasons is the lack of appropriate experimental datasets that could be used to develop a conceptual framework for describing flow and turbulence in the wildfire environment.

Our overall objectives in this research are: (1) to investigate the properties of turbulence spectra over a surface during fire front passage (FFP) as compared to those before and after FFP, which allows us to directly measure the spectral energy generated by fire-induced turbulence; and (2) to revisit the validity of the surface layer similarity theory but with effects of fire dynamics coexisting with boundary layer turbulence. Since there is no other suitable conceptual framework related to the description of turbulence spectra from the surface layer with the presence of fire, this study represents an initial attempt to evaluate the applicability of similarity law in this type of environment.

2. Experiments and data description

Four field experiments were conducted between the years 2008 and 2010, each with its unique site and fire characteristics (Fig. 1 and Table 1). Time-series data from these four experiments are used in the subsequent analyses.

2.1. Experiment 1: grass fire in valley

This observational campaign was conducted during a vegetation management fire (prescribed burn) conducted by Cal Fire (California Department of Forestry and Fire Protection) on 7 October 2008 at Joseph D. Grant County Park (37°19′N, 121°42′W). The park is located in the Diablo Range approximately 6.5 km east of San José, California and 60 km east of the Pacific Ocean. The experimental site is located in a northwest-southeast oriented valley, with the valley bottom elevation of 440 m above Mean Sea Level (MSL) surrounded by ridges that rise 660 m on the west and 830 m on the east. A detailed description of the site is discussed in Seto and Clements (2011). The burn unit was 0.14 km^2 (35 acres) in size, dominated by grass fuels including Italian Rye (*Lolium multiflotun*), Oat Grass (*Avena barbata*), Soft Brome (*Bromus hordeaceus*), and Purple Needle Grass (*Nassella pulchra*). The soils were dry and fuels were fully cured. The estimated fuel loading was 0.12 kg m^{-2} (0.5 tons $acre^{-1}$). Burn operations initially started as backing fire (a fire set along the inner edge of a fireline to consume the fuel in

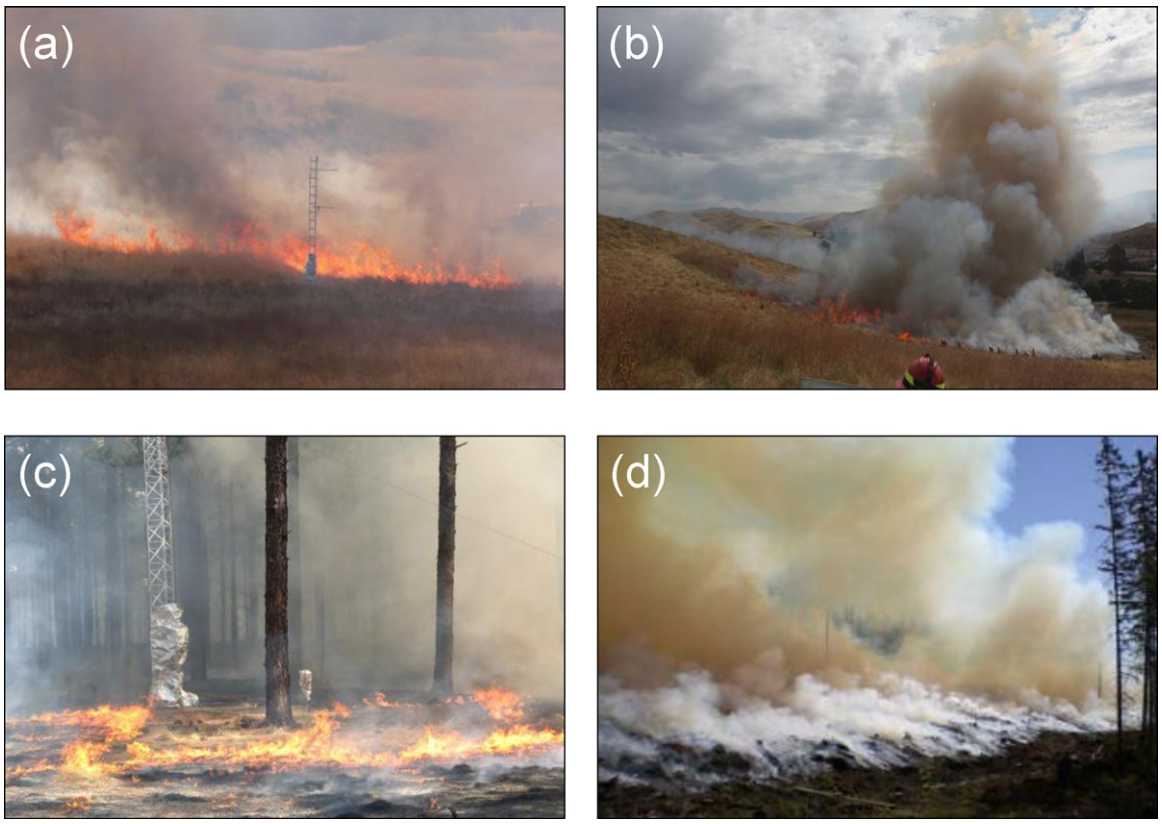

Fig. 1. Photographs of fire front, plume, and instrument tower within burn perimeter during (a) EXP1 at Joseph D. Grant County Park, CA; (b) EXP2 at Camp Parks, CA; (c) EXP3 at Calloway Forest, NC; and (d) EXP4 at Hyytiälä, Finland (Photo by Stylianos Kazantzis). Descriptions of each experimental burn are summarized in Table 1.

the path of a fire), but morning valley winds were replaced by the afternoon sea breeze minutes before the fire front passage at the tower, which drove the fire as head fire (a fire spreading with the wind). To capture the micrometeorology of the passing fire front, a 6.7 m guyed, steel tower was deployed near the center of the burn unit and the fire front was allowed to burn directly underneath as a head fire (a fire that moves in the direction of the wind). Low relative humidity (25–40%) and clear skies were observed throughout the experiment.

2.2. Experiment 2: grass fire on slope

The Grass Fires on Slopes Experiment was conducted on 24 June 2010 at the Camp Parks Reserve Forces Training Area (37°43′N, 121°52′W, 128 m MSL) located near Dublin, California and ~50 km north-northwest of Experiment 1 site. The primary goal of this experiment was to determine the role of fire–atmosphere interactions on fire behavior during a head fire running upslope. In situ measurements were made with a 12 m micrometeorological tower placed in the middle of a 250 m-long, north northwest-south southeast oriented 20° slope. The hill height is approximately 50 m and several hills and ridges with similar heights are also surrounding the site. The burn unit was approximately 0.02 km^2 (5 acres) in size, with fully cured tall grass similar to experiment 1 site mentioned above. Problems arose when the winds did not allow for upslope fire spread and therefore, the fire was ignited across the slope in a complicated ignition pattern with multiple ignition lines. The prevailing wind direction was from the west (cross slope) at 7 m s^{-1}. The atmospheric boundary layer during the experiment was characterized by high relative humidity (70–88%) and moderate to strong sea breeze. Skies were mainly cloudy before the ignition due to the wide spread stratus over the area, becoming partly cloudy during the burn. Ignition started at 0900 LT and the burn was completed by 1000 LT. The instruments became inoperable ~10 min after the FFP at the tower due to the power cable damage. A post-FFP data were collected for about 20 min after the power recovery at 1020 LT.

Table 1
Summary of the experimental site, burn operation, instrument height, and observed maximum sonic temperature and total heat flux for the experimental burns (a)–(d) as shown in Fig. 1.

	a (EXP1)	b (EXP2)	c (EXP3)	d (EXP4)
Site	CA	CA	NC	Finland
Burn date	October 7, 2008	June 24, 2010	March 7, 2010	June 26, 2009
Terrain	In a valley	Hill	Within canopy	Flat
Burn size in km^2 (acres)	0.14 (35)	0.02 (5)	0.25 (61)	0.01 (2.5)
Fuel type	Grass	Grass	Long leaf Pine litter	Timber Slash
Type of burn	Head	Head	Back	Back
Sonic anemometer height (m AGL)	6.7	11	3	12
Radiometer height (m AGL)	5	1	1	1
Measured maximum sonic temperature (°C)	157.8	201.0	202.5	196.8
Measured maximum total heat flux (kW m^{-2})	12.3	122.7	50.2	42.9

Since the post-FFP data is shorter than other blocks, the spectrum is not calculated.

2.3. Experiment 3: low-intensity fire within canopy

A comprehensive field program was conducted during a prescribed sub-canopy burn in The Nature Conservancy's Calloway Forest (35°01′N, 79°17′W, 130 m MSL), in North Carolina during March 2010. The primary objective of the research was aimed specifically at low intensity and smoldering fire for studying smoke emissions, transport, and dispersion properties within canopies. Observational data were collected using a 23 m (75 ft) guyed, aluminum tower in a uniform ~80-year-old stand of 18–20 m long-leaf pine (*Pinus palustris* Mill.) forest with sandy soil on relatively flat terrain. A mixture of 1-h and 10-h fuels of longleaf pine litter, turkey oak and wiregrass were the primary fuels on the ground in the burn unit (Unit 14) where 0.25 km^2 (61 acres) were burned with a backing fire. Ignition started at 1120 LT from the northeastern corner of the burn unit and the flaming phase of the burn was over at 1520 LT. Low relative humidity (20% before the ignition; 13% during the burn) and light southwesterly winds were observed within the canopy, although stronger winds were present at the canopy top. Although the 20-m instrumented tower was deployed in a relatively open, gap-like area in the canopy to allow for the placement of guy wires, the measurements on the tower were assumed to capture the turbulence regime inside the forest vegetation layer.

2.4. Experiment 4: slash burn in flat terrain

Atmospheric measurements were carried out during the IS4FIRES Experiment conducted 26 June 2009 at Hyytiälä, Finland (Clements et al., 2009). The overall experiment objective was to develop an Integrated Monitoring and Modelling System (IS) for wildland fires (IS4FIRES). The field measurement campaign included an extensive array of gas and particulate samplers located at the SMEAR II (Station for Measuring Forest Ecosystem – Atmosphere Relations: http://www.mm.helsinki.fi/hyytiala/) site (61°51′N 24°17′E, 181 m MSL), augmented with additional sensors specific to this experiment. Aircraft measurements of aerosols and meteorological conditions within and downwind of the plume were also conducted. The site is located in boreal coniferous forest dominated by a nearly homogenous, 40-year-old Scots pine (*Pinus sylvestris* L.) stand. The experiment was designed to have the SMEAR II towers downwind of the burn unit in order for the smoke plume to impinge on the instrument arrays. The burn unit was cut in February 2009 and was approximately 0.01 km^2 (2.5 acres) in size with a circular shape. A 12-m tree left standing in the slash within the burn unit was used as a measurement platform. Ignition started at 0750 LT on the north side of the circular burn plot and continued in both clockwise and counter clockwise directions around the plot. The in situ observational data were collected until 0940 LT when the ignition was completed on the southeast side of the plot while there were still smoldering fuels. Unfortunately, turbulence data were not collected long enough after the burn to calculate the post-FFP turbulence statistics and spectra. Hereafter, we reference the Experiments 1–4 as EXP1–EXP4, respectively.

2.5. Instrumentation

In situ high-frequency velocity and temperature data were collected at each of the above four sites using the same instrumentation but at different measurement heights. All turbulence measurements were made using a 3-D sonic anemometer (Applied Technologies, Inc., Sx-probe) sampled at 10 Hz, and theinstantaneous data were recorded using a Campbell Scientific, Inc. CR3000 datalogger mounted near the base of the tower housed in an environmental enclosure. The ATI Sx sonic anemometer performed very reliably under the extreme temperature environment of FFP and did not malfunction during or after the FFP. The ATI Sx probe was chosen since it was the only sonic anemometer commercially available with a custom calibration beyond 100 °C.

Total heat flux emitted from the fire front was measured using a Schmidt-Boelter heat flux sensor (Hukseflux, SBG01) in order to determine the fire intensity at the time of the FFP. However, the sensor was mounted near the sonic anemometer height looking downward during EXP1 and was placed above the ground facing horizontally during EXP2, EXP3, and EXP4. It is stressed that the measured total heat fluxes should be considered as reference values and not a true representation of the fire intensity due to non-linear nature of fires. An array of fine-wire thermocouples sampled at 1 Hz was also used to measure plume and near-surface temperature profiles. The datalogger and the base of the tower were protected from the extreme heat generated by the fire using fireproof insulation material wrapped around the lowest 2 m of the tower. Additionally, some fire resistant sheathing was used to protect the instrument cables. The sonic anemometer and total heat flux sensor heights are summarized in Table 1 along with the burn plot information.

2.6. Data processing

The time series data of wind velocity and sonic temperature were divided into three periods: pre-, during-, and post-Fire Front Passage (FFP) data. The during-FFP block was selected first so that the center of the 30-min block (18,000 data points) matched the time-series sonic temperature peak. The sonic temperature remained well above the ambient temperature over 30 min during EXP4 due to the circular ignition pattern, so multiple spectral outputs were averaged to produce a single during-FFP spectral curve. For this study, the 30 min block size was chosen to capture both fine-scale turbulence and larger eddies generated by fire–atmosphere interactions. The same time window was applied to the velocity time series data to define during-FFP velocity data. Next, pre- and post-FFP sections were selected as before and after the during-FFP periods and limited to daytime periods, since it has been shown that spectra under stable conditions (i.e. nighttime) are different from those under daytime convective conditions (Kaimal and Finnigan, 1994). The pre- and post-FFP periods were subsequently divided into several 30-min runs for the block averaging procedure performed later. This 30-min block-averaging has been used by several investigators (e.g. Van Gorsel et al., 2003; Zhang et al., 2010; Katurji et al., 2011) to study boundary layer turbulence structure, and it also removes the effect of the diurnal cycle and mesoscale phenomena (Nelson et al., 2007). A despiking routine was then performed to remove erroneous spikes in each 30-min block in pre- and post-FFP periods. Spikes that were four times the standard deviation within a 2-min moving window were replaced by linearly interpolated values. Unrealistic spikes in the during-FFP blocks were visually inspected, removed and replaced since the FFP period is a special circumstance of high turbulence levels associated with exceptionally strong surface heating (Lee et al., 2004). The horizontal wind velocities were rotated into streamwise (prevailing wind direction) and crosswise (perpendicular to streamwise direction) velocities u and v, respectively, and the vertical velocity w was tilt-corrected following Wilczak et al. (2001) in order to remove any bias of the anemometer mounting not being precisely level during deployment. The sonic temperature was not corrected for humidity, as the influence of the humidity variation on the sonic temperature is believed to be small and the effect does not change the overall magnitude of the results.

Caution is needed in calculating the during-FFP velocity and temperature perturbations from the block-averaged mean values because the 30-min block containing the FFP will be characterized by a mean velocity and mean temperature that may be quite different than the mean velocity and mean temperature during 30-min periods before and after the FFP. Consequently, the computed velocity and temperature perturbations during the FFP may not be a true reflection of the fire-induced perturbations. In this study, the during-FFP velocity and temperature perturbations were calculated from the 30-min block average mean one block prior to the during-FFP block, so that the calculated during-FFP perturbations are more representative of the fire-induced turbulence.

Wind velocity and temperature power spectra were computed using a continuous wavelet transform (complex Morlet) following Torrence and Compo (1998). Wavelet transforms are mathematical techniques based on group theory and square integrable representation and they use analyzing function called wavelets, which are localized in space, to decompose signals into space and scale (see Farge, 1992 for details). Wavelet analysis provides a better smoothed global spectral estimates than Fourier power spectra without involving binning and smoothing routines as demonstrated by Hudgins et al. (1993).

The individual wind velocity and temperature spectra were normalized by the friction velocity u_* and the scaling temperature T_*, respectively, and those parameters are defined as

$$u_* = [(\overline{u'w'})^2 + (\overline{v'w'})^2]^{1/4} \quad (1)$$

$$T_* = -\frac{\overline{w'T'}}{u_*} \quad (2)$$

where u', v', w', and T' are fluctuations of streamwise, crosswise, and vertical velocity and sonic temperature from the block-average value of the each variable, respectively. The $\overline{v'w'}$ term is included in u_* to take into account the possibility that the stress tensor may not be aligned with the mean wind (Roth and Oke, 1993). The normalized spectra were averaged into a single curve of the pre- and post-FFP for each burn and the during-FFP for EXP4. The frequency of each curve was normalized by z/U, where z is the measurement height and U is mean horizontal wind speed measured at the height z.

3. Results and discussion

3.1. Influence of fire front on turbulence statistics and spectra

3.1.1. Observed variances and turbulence intensities

Variances of wind velocity indicate the physical fluctuation intensity associated with velocity perturbations from the mean (Katurji et al., 2011). Studies of variances and spectra in the ABL provide a direct test of similarity predictions. The 30-min averaged variances are presented in Table 2. The horizontal variances during the FFP are largest during the EXP1. However, the valley wind-sea breeze reversal that occurred a few minutes before the FFP is the likely cause of these large variance values, as described in Seto and Clements (2011). Nonetheless, increased horizontal velocity variances during the FFP are evident for all other fires in Table 2 as a result of increased mean winds. This is not surprising since several other observations (Coen et al., 2004; Clements et al., 2007) confirm 2–3 times stronger horizontal wind speeds at the time of fire front passage than the background ambient winds due to fire-induced circulations. The increased mean wind during EXP3 also suggests that fire-induced flow can occur even within canopies. All four fires indicate increased vertical velocity and temperature variances as well as friction velocity u_* and scaling temperature T_* as a result of increased heat flux of the fires.

The observed temperature variances reflect the influence of ambient winds on each fire. The during-FFP temperature variances during EXP3 and EXP4 indicate larger values than those during EXP1 and EXP2. It is evident that the weak ambient mean winds, high turbulence intensities defined as σ_u/U, σ_v/U, and σ_w/U (Table 2), and locally very unstable conditions (Table 3) are favorable for vertical heat transport and resulted in the high temperature variances during EXP3 and EXP4. Similar turbulence intensity, yet stronger mean wind during EXP1 combined with the lower heat flux may have yielded lower temperature variance than those observed during EXP3 and EXP4. It is interesting to see that, despite the fact that the largest observed maximum temperature and heat flux occurred during EXP2, temperature variance during the FFP is considerably smaller during EXP2 as compared to those during the other burns. This is because the fire spread rather quickly at the tower under the strong mean wind combined with the effect of sloped terrain, both of which tend to accelerate fire spread. The strong mean wind and weak turbulence intensities also prevented hot smoldering plume from reaching the sonic anemometer at 12 m AGL after the FFP. As a result of the short duration of above-ambient temperature, the temperature variance calculated over 30 min period appeared small.

The variances shown in Table 2 suggest that the fire fronts generate turbulence in both the horizontal and vertical velocity components due to the increased mean winds around the fires known as fire-induced winds. Increased variances during the FFP were also observed by Clements et al. (2008) during the FireFlux experimental grass fire. The observations of the velocity variances indicate that fire-induced winds increased turbulence intensities of the horizontal velocity components during EXP2. Decreased turbulence intensities in crosswise velocity component were found during EXP3 and EXP4 with no change in turbulence intensity in streamwise velocity during EXP3, despite the fact that the fire-induced winds were observed. The increased variances during the FFP also result in increases in turbulence kinetic energy (TKE), $e = 1/2(\sigma_u^2 + \sigma_v^2 + \sigma_w^2)$. The contributions of horizontal velocity variances to the TKE are greater for all cases during the FFP. However, the decreased degree of anisotropy in TKE is evident when the fires passed through the towers. The ratio of the horizontal velocity variances to the vertical velocity variance observed during the EXP2, EXP3, and EXP4 experiments decreased during FFP as compared to the ratios of those observed before and after the FFP as seen in Table 2. The ratios range from 2 to 7 before and after the FFP, similar to the observations by Yadav et al. (1996) in unstable conditions. The ratios range from 1 to 4 during the FFP, with the largest anisotropy found within the canopy. Although the contribution of the vertical velocity variances to TKE increased during the FFP, the turbulence field remained anisotropic.

The dimensionless variances of the vertical velocity σ_w/u_* and temperature σ_T/T_* are presented as a function of the stability parameter z/L in Fig. 2. The similarity hypothesis of Monin–Obukhov suggests that after nondimensionalization, flow properties are functions only of z/L, and the relationships between the dimensionless variances of w and T with z/L in the surface layer are described as $\sigma_w/u_* = \phi_w(z/L)$ and $\sigma_T/T_* = \phi_T(-z/L)$, respectively, where ϕ_w and ϕ_T represent universal functions. Wyngaard et al. (1971) showed a behavior of local free convection as a $(-z/L)^{1/3}$ trend for the nondimensional vertical velocity variance with $\phi_w = 1.9$ at large negative z/L (i.e. $z/L \ll -1$) and a $(-z/L)^{-1/3}$ trend for the nondimensional temperature variance with $\phi_T = 0.95$ at large negative z/L. In this case, turbulent quantities of velocity and temperature are substantially independent of u_* and T_*. The local free convection similarity is useful for statically unstable surface layers where buoyancy is the driving force behind the turbulence (Stull, 1988). Since the large sensible heat produced by FFP, a scaling similarity is assumed to approach free convective

Table 2
Values of 30-min averaged horizontal mean wind speed U (m s^{-1}), friction velocity u_* (m s^{-1}), scaling temperature T_*, variances of u, v, and w (m^2 s^{-2}), and temperature (K^2), normalized variances $\sigma_{u,v,w}/u_*$, and turbulence intensities $\sigma_{u,v,w}/U$ observed at each site.

		a (EXP1)	b (EXP2)	c (EXP3)	d (EXP4)
U	Pre	2.33	6.86	1.05	1.06
	During	3.33	7.21	1.78	2.58
	Post	3.66	6.29	1.05	
u_*	Pre	0.29	0.58	0.20	0.26
	During	0.53	0.89	0.31	0.65
	Post	0.39	0.67	0.22	
T_*	Pre	0.61	0.11	0.50	0.42
	During	1.85	5.70	7.21	6.21
	Post	0.60	0.16	0.16	
σ_u^2	Pre	0.48	1.60	0.57	0.40
	During	6.21	2.96	1.65	2.89
	Post	1.33	1.93	0.53	
σ_v^2	Pre	0.47	0.93	0.60	0.35
	During	3.87	2.43	1.15	2.00
	Post	1.69	1.17	0.69	
σ_w^2	Pre	0.16	0.28	0.10	0.17
	During	0.44	1.27	0.41	1.84
	Post	0.34	0.41	0.10	
σ_T^2	Pre	0.62	0.04	0.44	0.18
	During	28.30	5.07	57.90	45.40
	Post	0.82	0.41	0.28	
σ_u/u_*	Pre	2.41	2.19	3.70	2.43
	During	4.70	1.93	4.14	2.62
	Post	2.99	1.93	3.35	
σ_v/u_*	Pre	2.38	1.67	3.78	2.27
	During	3.71	1.75	3.45	2.18
	Post	3.37	1.62	3.82	
σ_w/u_*	Pre	1.37	0.92	1.53	1.60
	During	1.25	1.27	2.07	2.09
	Post	1.51	0.96	1.44	
σ_T/T_*	Pre	1.29	1.82	1.33	1.01
	During	2.88	0.40	1.06	1.09
	Post	1.51	4.00	3.31	
σ_u/U	Pre	0.30	0.18	0.72	0.60
	During	0.75	0.24	0.72	0.66
	Post	0.32	0.22	0.69	
σ_v/U	Pre	0.30	0.14	0.74	0.56
	During	0.59	0.22	0.60	0.55
	Post	0.36	0.17	0.79	
σ_w/U	Pre	0.17	0.08	0.30	0.39
	During	0.20	0.16	0.36	0.53
	Post	0.16	0.10	0.30	

conditions for $z/L \ll -1$. The normalized vertical velocity variance measured during FFP in Fig. 2a show a fairly good agreement with the 1/3 slope for $z/L \ll -2$, although the observations can be better fitted with 1/2 power trend for $z/L \ll -1$ and suggest $\phi_w = 1.3$. On the other hand, the normalized temperature variances during FFP shown in Fig. 2b exhibited more scatter than the during-FFP normalized vertical velocity variances in Fig. 2a. The observations are better fitted with $(-z/L)^{-1/2}$ and $\phi_T = 1.4$ for $z/L \ll -1$ except for EXP2 in which the quick FFP followed by an effective temperature cooling due to the strong mean wind led to the small

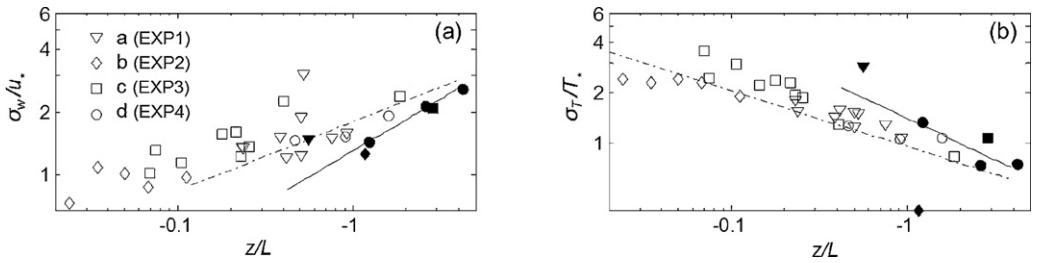

Fig. 2. (a) Normalized σ_w and (b) normalized σ_T as functions of z/L in unstable conditions. The hollow symbols indicate pre- and post-FFP data and the solid symbols indicate during-FFP data. The dashed line of the 1/3 slope $\phi_w = 1.9$ in (a) and $-1/3$ slope $\phi_T = 0.95$ in (b) are the local free convection prediction shown in Wyngaard et al. (1971). The solid black line represents 1/2 slope with $\phi_w = 1.3$ in (a) and $-1/2$ slope $\phi_T = 1.4$ in (b).

Table 3
Summary of the stability parameter z/L before, during, and after the FFP for the experimental burns (a)–(d) as shown in Fig. 1.

		a (EXP1)	b (EXP2)	c (EXP3)	d (EXP4)
z/L	Pre	−0.65	−0.06	−0.24	−0.99
	During	−0.56	−1.17	−3.07	−2.69
	Post	−0.37	−0.06	−0.17	–

during-FFP temperature variance. The departure of both normalized variances from the expected scaling of Wyngaard et al. (1971) could be caused by the fact that the local free convection similarity approach is appropriate for surface layers in calm mean wind conditions. The environment of FFP tends to increase mean winds as shown in Table 2 and thus the local free convection prediction may not be verified. It is emphasized that time dependence of temperature during the FFP strongly influences the temperature scaling demonstrated here as the variances used in the similarity scaling always involve time-averaged perturbations of velocity and temperature. The applicability of similarity scaling on turbulence spectra is investigated further in Section 3.2.

3.1.2. Horizontal velocity spectra

To assess spectral behavior in the surface layer during the FFP at the instrumented tower, we compare observed spectra during FFP with those before and after the FFP. In order to facilitate the direct comparison of magnitudes, the velocity and temperature spectra, as well as the frequency of the spectra, have not been normalized for this discussion. The streamwise velocity spectra are presented in Fig. 3. All pre- and post-FFP spectra approach a −2/3 slope quite well at high frequency as suggested by Kolmogorov theory (Kolmogorov, 1941), showing a property of the inertial subrange. In addition, the isotropic ratios between vertical and streamwise velocity components for EXP1–EXP4 are presented in Fig. 4. In the surface layer, eddies in the inertial subrange are isotropic and Kolmogorov's inertial subrange law requires $S_w/S_u = 4/3$ to be locally isotropic. The requirement is fulfilled for Fig. 4a, b, and d as the ratios approach 4/3. Within the canopy, local isotropy is generally violated (Kaimal and Finnigan, 1994). The observed ratio within the canopy in our study (Fig. 4c) approaches 1 and is in good agreement with the observed value of Amiro (1990) for a pine forest, indicating that our measurements are representative of the actual turbulence regime inside the forest vegetation layer. The during-FFP spectral curve on each burn exhibit several unique features that are not observed in the pre- and post-FFP spectra. The during-FFP spectra in Fig. 3a–c contain increased energy at high frequency, while Fig. 3d shows the increased spectral energy throughout the entire frequency range. As a result of the enhanced high-frequency contribution, the behavior of the inertial subrange seems to deviate slightly from the −2/3 roll-off slope for the during-FFP spectra. Since there is no energy production or dissipation in the inertial subrange, the increased energy in this region could be produced directly by high frequency horizontal motions due to fine-scale eddies and entrainment of air generated by the fire. Wieser et al. (2001) found that the lee wakes developing downwind of an obstruction (sensor component in their case) can be resolved by sonic anemometers and they clearly appear at the high-frequency end of the velocity spectrum. Fine-scale, fire-induced eddies are likely responsible for the observed high frequency variations in the winds, similar to the effect of the wakes as observed by Wieser et al. (2001).

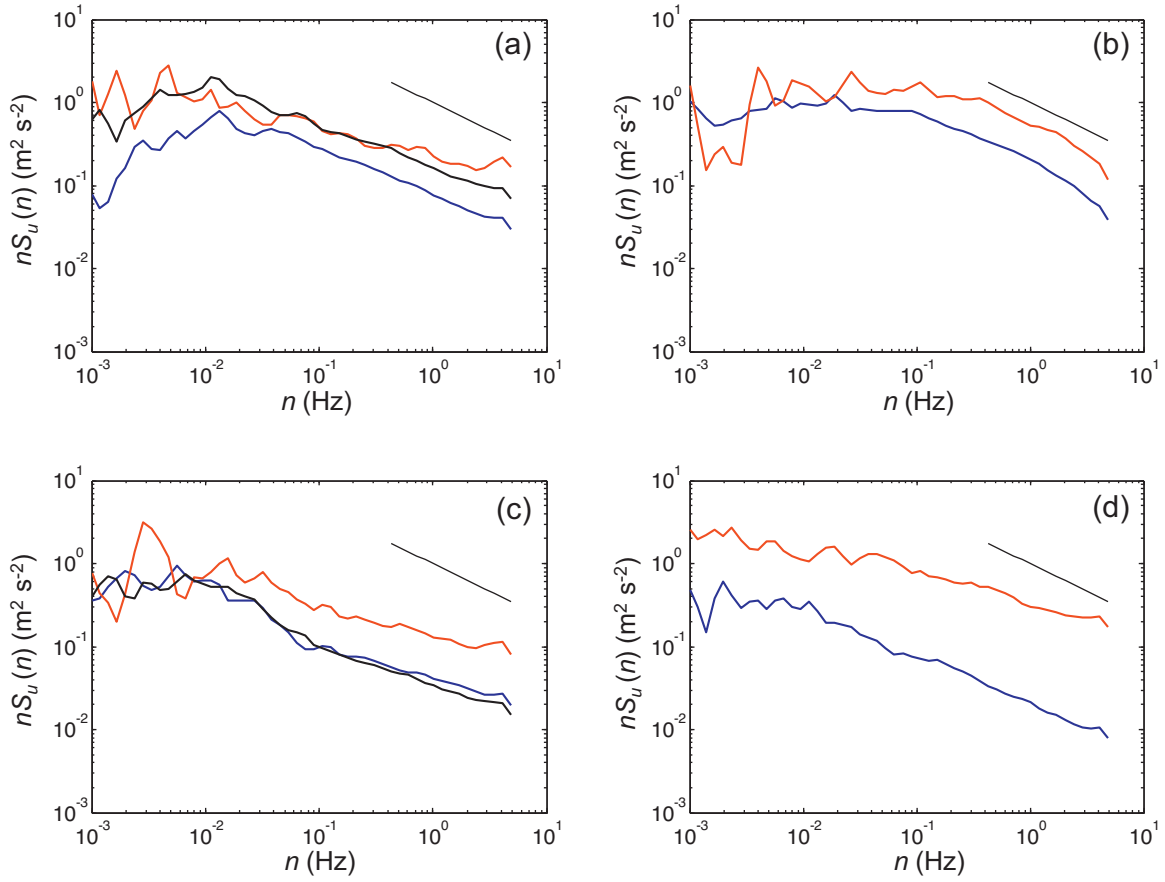

Fig. 3. Non-normalized power spectra of the streamwise wind velocity $nS_u(n)$ as a function of the natural frequency n for the experimental burns (a)–(d) as shown in Fig. 1. Short line represents -2/3 slope of inertial subrange. Pre-, during-, and post-FFP spectra are shown in blue, red, and black, respectively. (For interpretation of the references to color in this figure legend, the reader is referred to the web version of the article.)

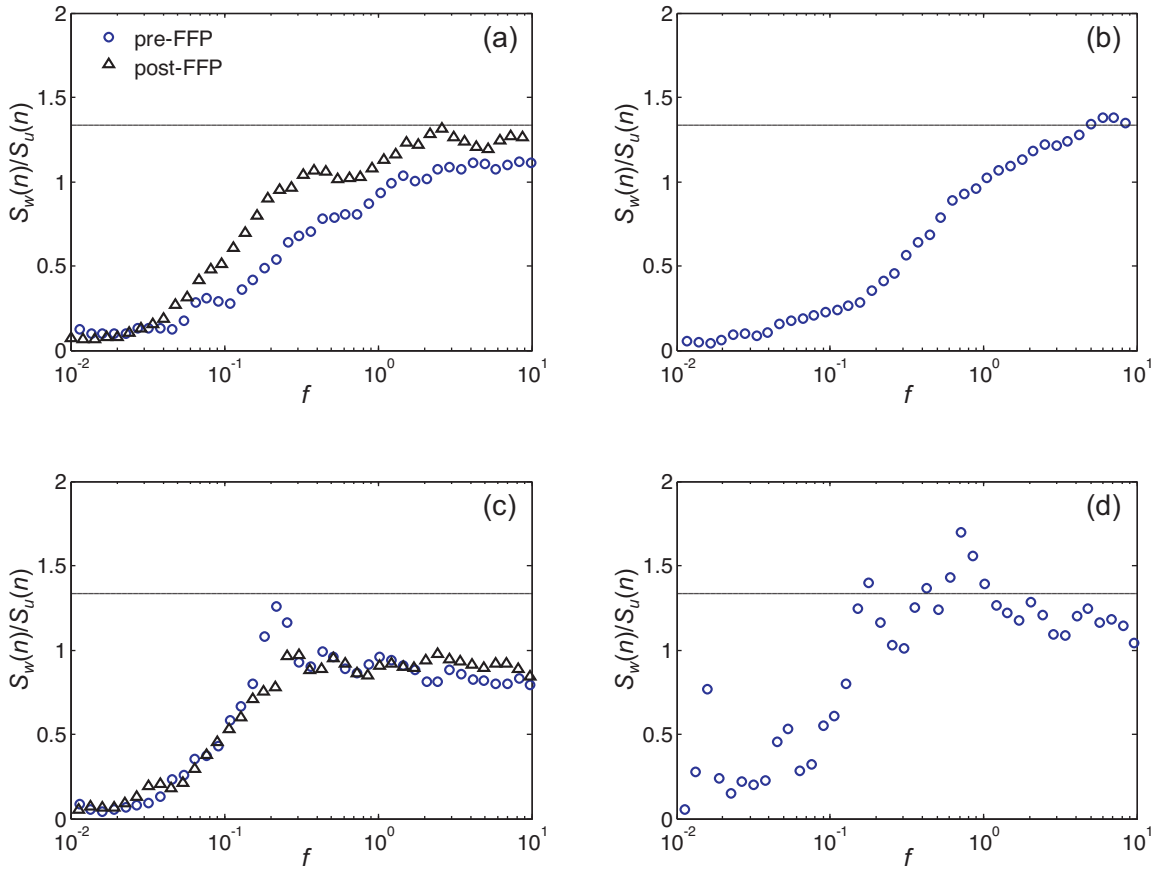

Fig. 4. Ratios of vertical to streamwise power spectra as a function of the normalized frequency, $f = nz/U$ for the experimental burns (a)–(d) as shown in Fig. 1. Pre- and post-FFP spectra are shown with circles and triangles, respectively. The ratio of 4/3 is indicated by a dashed line to allow for assessment of isotropy.

Extending the discussion further, the increased spectral energy over the inertial subrange during the FFP as shown in Fig. 3 can be explained from the results of laboratory scale fire–wind analysis. Weckman and Strong (1996) investigated the turbulence structure of a 31-cm diameter methanol pool fire and demonstrated that the autospectral densities calculated from measured radial and axial velocities showed the spectral peaks corresponding to an eddy frequency of 2.8 Hz. In fact, the frequency of formation and departure of the outer eddies from the base of the plume, called vortex shedding, and its frequency f in Hz for the fire diameter D in meters is approximately $f = 1.5/D^{1/2}$ (Quintiere, 1998). Wildfires would shed eddies at much lower frequencies than those observed in laboratory scale fires, since D is much larger than laboratory pool fires. For example, a 100-m diameter circular burning area should shed vortices with characteristic frequencies of around 0.15 Hz. But even so, this vortex shedding frequency is perhaps constrained to above the mid-frequency range of the atmospheric turbulence. Consequently, the scales of eddies generated by fire seem to coincide with the inertial subrange of the atmospheric surface layer spectra shown in Kaimal and Finnigan (1994). The vortex shedding frequency seems to depend upon the fire intensity that varies with time, so it should appear in a wide range of a spectrum. Although the fire front intensity, the magnitude of heat transfer, and turbulence effects involved at the laboratory scale are typically not comparable to those in the field, the vortex shedding frequency can be used to provide a range of plausible values. The turbulence spectra of laboratory-scale fires appear to have a $-5/3$ inertial subrange slope above 1 Hz. The fire fronts passed the in situ towers during our experimental burns as line fires except for EXP4; yet, laboratory-scale experiments show that pool fires have qualitatively similar characteristics as line fires (Quintiere, 1998). Based upon the assumption that the scales of eddies shed by fires depend primarily on the heat source intensity, it is proposed that fire–atmosphere coupling is necessary in order to generate larger eddies that appear below the vortex shedding frequency of the fire.

The passage of the fire front within the canopy resulted in an increased u velocity spectra above 0.01 Hz (Fig. 3c) and v velocity spectra above 0.04 Hz (Fig. 5c). Although a spectral peak is seen in the energy-containing range for u and v velocity spectra, energy increase is more pronounced in mid to high frequencies in both spectra. Thus, the increased high-frequency energy is attributed to eddies that are somewhat smaller than the low frequency, energy-containing ambient eddies. This is because the turbulent energy is produced differently within the canopy than over flat and homogeneous terrain. According to Finnigan (2000), within the canopy the dominant large eddies are produced by shear at the top of the canopy due to an inviscid instability of the inflected mean velocity profile, whereas over flat, uniform terrain the bulk of the turbulent energy within the surface layer is produced by strong shear and buoyancy. Unless the mean wind profile above the canopy is affected by the fire as observed during grass fires where downward motion occurs behind the fire front bringing down higher momentum from aloft (Clements et al., 2007), the spectral energy in the energy-containing range is not expected to change. Since the sub-canopy burn was such a low intensity, it is unlikely that the fire affected the mean wind profile above the canopy. In addition, Finnigan (2000) notes that the major contributor to momentum transfer within and just above the canopy is dominated by sweeps, the penetration of the canopy by fast, downward moving gusts. The updraft produced by the fire, in contrast, may counteract

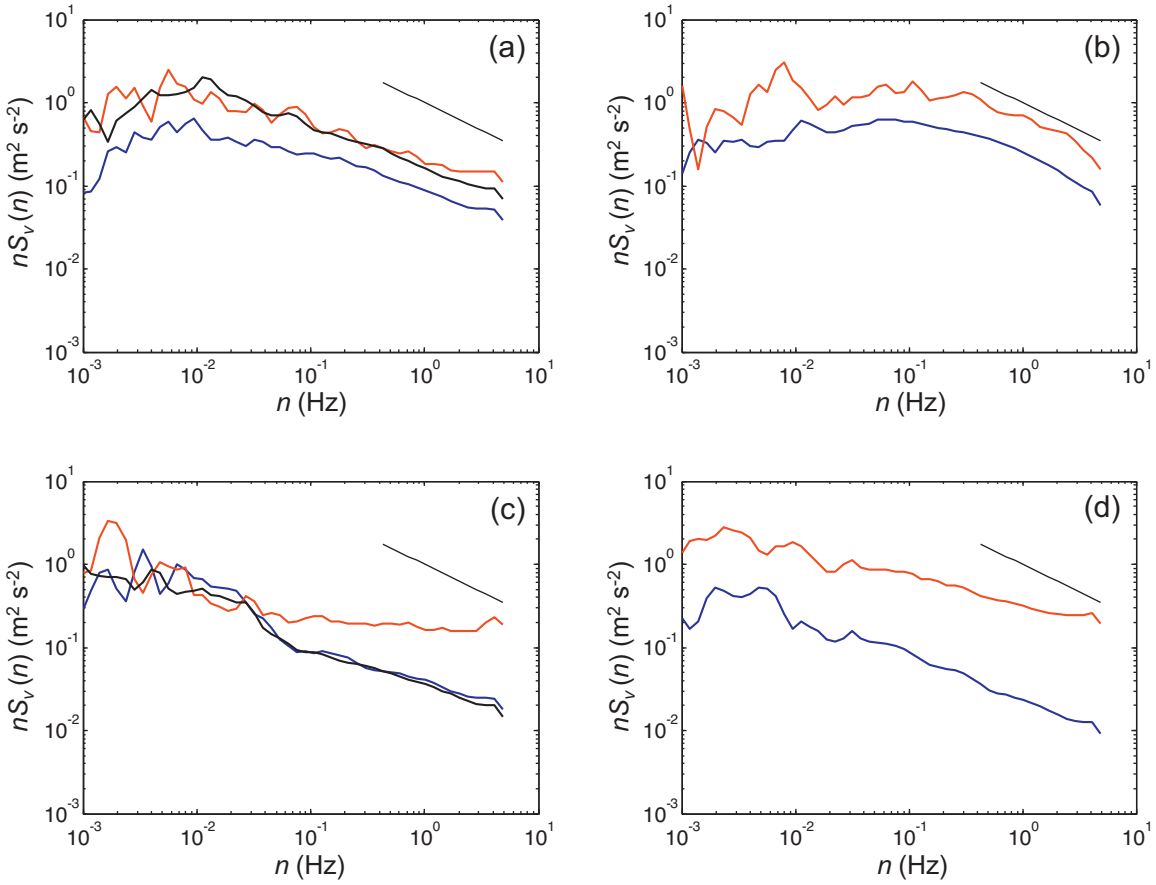

Fig. 5. Non-normalized power spectra of the crosswise wind velocity $nS_v(n)$ as a function of the natural frequency n for the experimental burns (a)–(d) as shown in Fig. 1. Short lines indicate −2/3 slope of inertial subrange. Pre-, during-, and post-FFP spectra are shown in blue, red, and black, respectively. (For interpretation of the references to color in this figure legend, the reader is referred to the web version of the article.)

the sweeps especially above the heat source, perhaps causing the reduction of the downward momentum transfer. As a result, spectral energy at the lower frequency range in the horizontal velocity components could even decrease during the FFP as seen in the low frequency sides of Figs. 3c and 5c. The increased mean wind speed without a substantial energy increase in the energy-containing range within the canopy on the other hand, suggests that small scale turbulence perhaps influenced the mean wind profile under the canopy. It is also noted that a marked secondary maximum in the mean wind speed was observed around $z/h = 0.12$, where h is the canopy height, within a Douglas-fir stand by Lee and Black (1993), close to our measurement height $z/h = 0.15$. Around the height, a trunk space is relatively free of branches, allowing for less restricted air movement. Since they found that the second maximum wind speed was least coupled with the wind speed above the stand, it is hypothesized that the fire influenced the secondary maximum wind speed. Overall, the effect of the canopy combined with a low-intensity fire greatly inhibited formation of the large, energy-containing eddies and roll vortices generated by fire–atmosphere coupling (i.e., Jenkins et al., 2001). While the primary reason for the increased spectral energy at high frequency is perhaps small eddies produced by convection and entrainment associated with the fire and plume, it is also evident that the high frequency turbulence energy was generated partly due to the low-level wind shear within the canopy as suggested by the increased mean wind speed measured at 3 m AGL during the FFP (Table 2). Detailed interactions of the high-frequency turbulent energy produced by the fire with the aerodynamic drag of the foliage are not a primary focus in this study. Based upon our visual observations of the enhanced foliage motions during the FFP, however, their contribution to the high frequency energy may be large as the kinetic energy of the increased mean flow within the canopy should be converted directly into fine-scale turbulence in the wakes of canopy elements (Finnigan, 2000).

Clearly shown in Figs. 3d and 5d is the increased spectral energy in the horizontal velocity components over the entire frequency range during EXP4. A circular ignition pattern over the logging slash fuel under the light ambient winds led the fire behavior to a convection-driven regime near the center of the burn area, where the instruments were located. Even though the experimental burn plot was surrounded by a boreal coniferous forest, the trees were far enough away from the measurement platform and the clearing was sufficiently large that the turbulence characteristics were unaffected by the canopy during the fire. It is hypothesized that the strong fire–atmosphere coupling caused the increases in the low frequency energy (energy-containing large eddies) in the horizontal velocity spectra.

3.1.3. *Vertical velocity spectra*

All vertical velocity spectra presented in Fig. 6 show well-defined peaks in the mid-frequency range, when compared with the horizontal velocity spectra. In fact, the spectral peak frequencies during FFP are similar to those before and after the FFP, although the peaks are less pronounced during the FFP. All during-FFP spectra suggest that the increased vertical velocity variance presented in Table 2 was caused by the increased energy from low and high frequencies.

The post-FFP vertical velocity spectrum for EXP1 (Fig. 6a) shows increased spectral energy at all frequencies as compared with the pre-FFP spectrum. The higher post-FFP mean wind speeds are

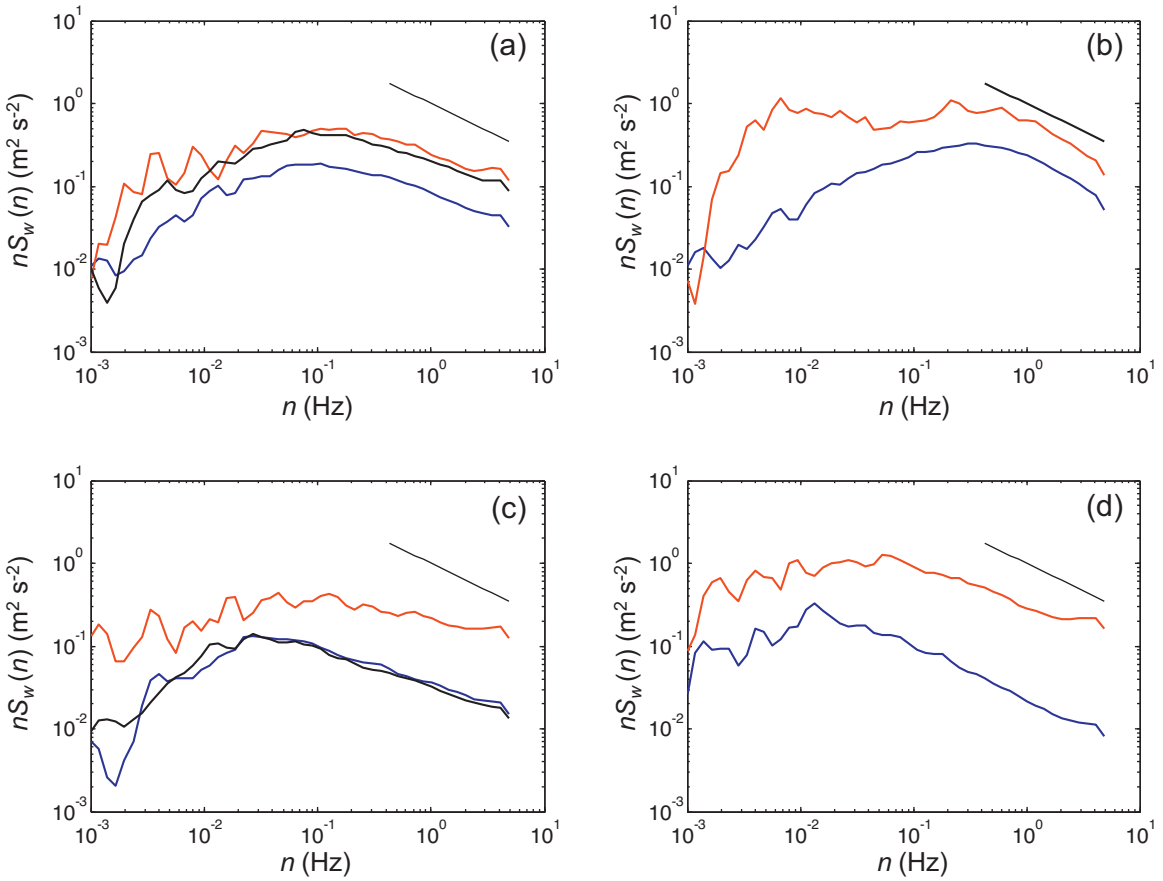

Fig. 6. Non-normalized power spectra of the vertical wind velocity $nS_w(n)$ as a function of the natural frequency n for the experimental burns (a)–(d) as shown in Fig. 1. Short line represents -2/3 slope of inertial subrange. Pre-, during-, and post-FFP spectra are shown in blue, red, and black, respectively. (For interpretation of the references to color in this figure legend, the reader is referred to the web version of the article.)

associated with a sea breeze intrusion into the valley. This feature is consistent with the horizontal velocity spectra (Figs. 3a and 5a), although the increased energy is much smaller in the vertical velocity component than the horizontal velocity components. However, the valley wind–sea breeze interaction resulted in increased variances only in the horizontal velocity components as discussed in the previous section, and the vertical velocity variance in Seto and Clements (2011) shows little change during the wind shift. Thus, the increased spectral energy associated with the convective eddies generated by the fire front is rather small, especially when compared with the post-FFP w spectrum. To explain the physical processes involved, existing numerical model results are used here for qualitative comparisons. In a series of two-dimensional simulations with extreme temperatures (900 K and 1500 K) associated with a heating line source, Heilman and Fast (1992) showed that ambient crossflows (mean winds that flow perpendicular to the heating lines) play a significant role in the development of buoyancy-induced horizontal roll vortices above the heating source. They demonstrated that, when sufficiently strong ambient crossflow is present, the development of the updraft and downdraft are inhibited above the heating region and no horizontal vortices form. This result is consistent with the concept of the convective Froude number (Clark et al., 1996); It suggests that when kinetic energy of the air associated with horizontal winds is sufficiently strong to overcome potential energy provided by the surface heating, fire–atmosphere interactions become negligible. The model simulations with the 900 K heating lines in Heilman and Fast (1992) are comparable with EXP1 (Seto and Clements, 2011) as the heat flux of 37 kW m^{-2} in the numerical setup is representative of the low-intensity fire of EXP1 with observed maximum total heat flux of ~12 kW m^{-2}. In addition, the 900 K heating line temperature represents the flame temperature for grass fires as Clements et al. (2007) observed the maximum fuel temperature of ~900 K. While Seto and Clements (2011) did not observe the flame temperature during EXP1, their observed maximum thermocouple temperature, T_c, of 120 °C at ~2 m AGL agrees very well with the observed T_c of Clements et al. (2007) at the same measurement height. By using the model simulation results of Heilman and Fast (1992) qualitatively, we hypothesize that the sea breeze had a strong influence in suppressing the vertical development of the convective column, as opposed to the influence of the fire's buoyant forcing. The z/L stability parameter also reflects this point as the value becomes more negative (unstable) during the FFP for EXP2–EXP4 as one may expect due to fire's strong surface heating, whereas EXP1 shows less negative z/L value during the FFP due to sea breeze that brought a cooler air into the valley. This resulted in the only small increase in the w spectral energy during the FFP in comparison with that after the FFP.

Our w spectra observed during EXP2 (Fig. 6b) suggest that large-scale eddies are considerably enhanced during the FFP. The w spectrum during the FFP shows a prominent peak at f = 0.007 Hz, which did not exist before the FFP, while the spectral peak observed around 0.3 Hz before the FFP remains at the same frequency during the FFP, resulting in the two predominant peaks or double peaked w spectrum. The v velocity spectrum during the FFP (Fig. 5b) also shows a peak at 0.008 Hz, which coincides with the secondary peak in the w spectrum developed during the FFP. On the other hand, the u velocity spectrum during the FFP shows increased energy

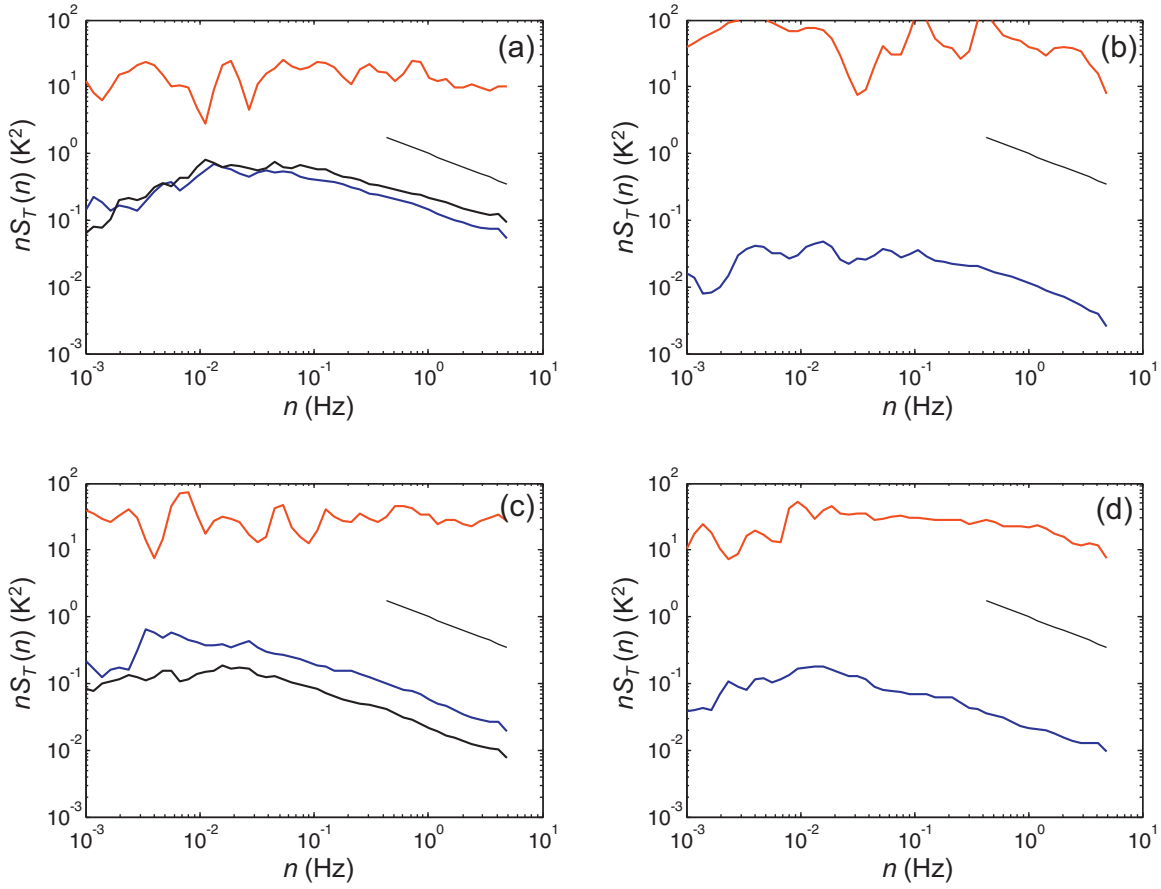

Fig. 7. Non-normalized power spectra of the temperature $nS_T(n)$ as a function of the natural frequency n for the experimental burns (a)–(d) as shown in Fig. 1. Short line represents -2/3 slope of inertial subrange. Pre-, during-, and post-FFP spectra are shown in blue, red, and black, respectively. (For interpretation of the references to color in this figure legend, the reader is referred to the web version of the article.)

toward the mid to high frequencies but not at the low frequency side. Since the v component of the velocity aligns with the slope axis of the local terrain, a possible explanation of the double-peaked w spectra is a development of a buoyancy-induced roll vortex over the slope as shown in the numerical simulation of Heilman (1992). Heilman (1992) simulated the circulation patterns and turbulence energy fields associated with various surface heating-line locations and ambient crossflow conditions on simple two dimensional hills. While the experimental conditions are different than the numerical setup in Heilman (1992) in that the simulations are designed to provide the two dimensional (upslope/downslope velocity components with height) circulation patterns and do not include the cross-slope wind component, cross-slope winds are the prevailing wind directions during EXP2. Heilman (1992) demonstrated that the presence of an ambient crossflow tends to reduce the magnitude and vertical extent of turbulent energy over heating lines on the leeward slope of a hill. We hypothesize that despite the strong cross-slope flow, weak vorticity did form above the burn plot on the slope and extend several hundred meters vertically to generate large eddies as suggested by the v and w spectra. The vertical length scale during the FFP was approximated using the peak frequency and mean vertical velocity. The lower frequency peak corresponds to 100 m, twice the height of the hill. Although the simulations of cross-slope burn are not available to confirm the effects of the cross-slope flow, the flow may have similar dissipative effects on the vorticity in the cross-slope direction as it can tilt the convective column and limit the vertical extent of the vortices. That is perhaps why the increase in u spectral energy during the FFP is less pronounced at the low frequency in comparison with the increase in v spectral energy (Figs. 3b and 5b). Nonetheless, the effects of the crossflow on the development of vortices seem to be important in driving fire behavior and in limiting the vertical extent of the turbulence.

The vertical and horizontal velocity spectra during the FFP within the canopy burn (Figs. 3c, 5c, and 6c) have very similar spectral behavior at high frequencies in that they show pronounced increased spectral energy with slightly slower roll-off slopes than the −2/3 inertial subrange slope that appears before and after the FFP. The increased high-frequency energy can be explained by the fact that low intensity fires such as in the sub-canopy burn produce weaker turbulence than large, intense fires as described in Section 3.1.2. In addition, it is possible that downdrafts transport fine-scale eddies generated by the interactions of convection and aerodynamic drag of the foliage downward into the vegetation layer, resulting in the high frequency energy enhancement. This physical process is similar to the spectral short cut described by Kaimal and Finnigan (1994) and Finnigan (2000). The aerodynamic drag of the foliage acts not only on the mean flow above the canopy but also on turbulent eddies of all scales larger than the canopy elements, causing the continual removal of energy from the eddy cascade and violating the fundamental assumption of Kolmogorov's −5/3 law for the inertial subrange. While Finnigan (2000) pointed out that sonic anemometers of 10–15 cm path length, such as the ATI Sx probe that we employed during the burn, have difficulty in resolving the dominant scales of wake kinetic energy (WKE) defined as the fine-scale wake component of TKE, the process is believed to contribute to the increased high frequency energy to some degree.

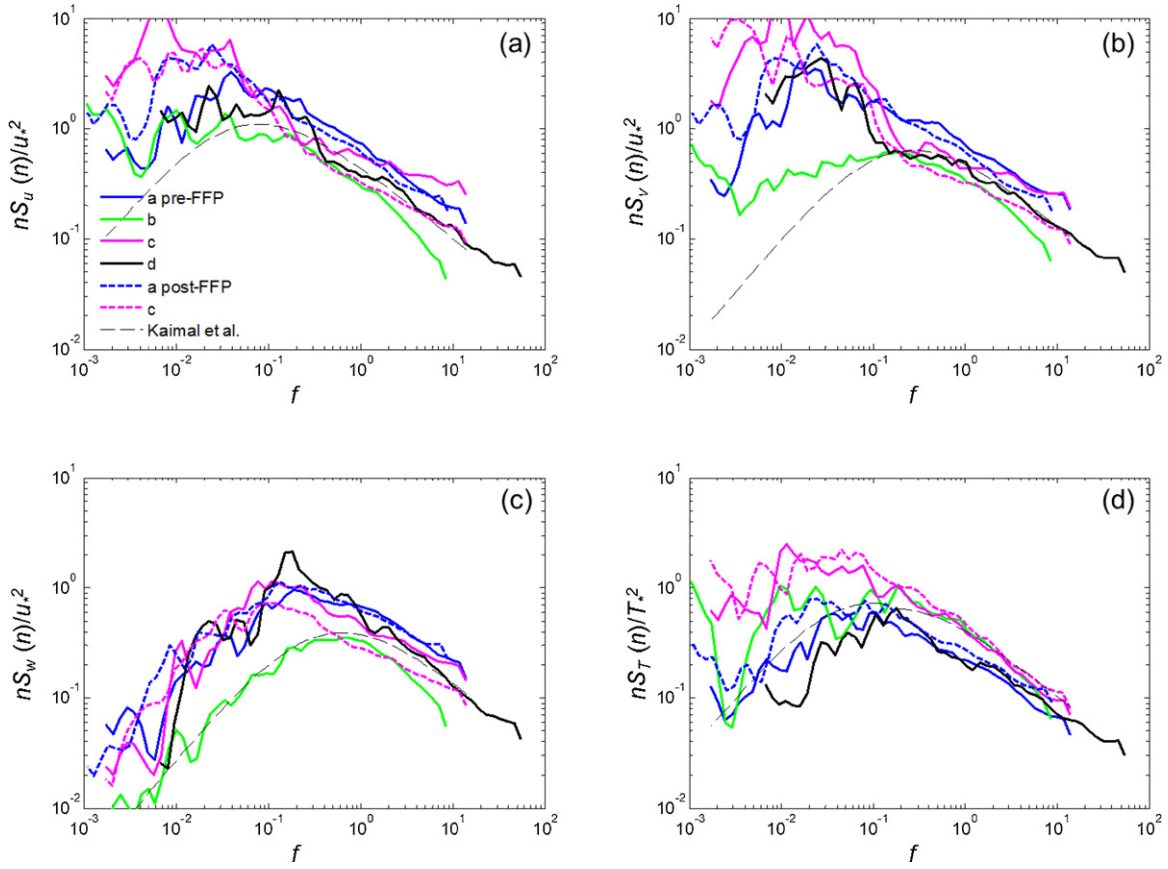

Fig. 8. Normalized spectra of velocity components and temperature observed before and after the FFP during the four experiments: (a) for u; (b) for v; (c) for w; and (d) for T as a function of the normalized frequency, $f = nz/U$. The dashed lines in the plots indicate the velocity and temperature spectra for neutral stability obtained by Kaimal et al. (1972).

In contrast to the similarity seen in the horizontal and vertical spectral behavior at higher frequencies during the FFP, the low frequency spectral behavior differ in that the w spectral curve during the FFP shows increased energy at low frequency, which did not occur in the horizontal velocity spectra during the FFP. One known effect of forest clearing is the air motion in the daytime that is directed toward the direction of the clearing as summarized in Lee (2000). It is possible that the clearing of branches above the tower site allowed for effective plume ventilation when the fire moved below the tower, resulting in the increased w spectral energy. The convergence enhanced by both the fire and the forest clearing also explains the observed increased mean wind speed within the canopy during the FFP.

The spectral characteristics of the measured horizontal and vertical velocities during the FFP were analyzed using the traditional surface layer spectral analysis. Although we need more field data that are complete and well documented for comparisons and analysis to draw solid conclusions about the energetics of fire fronts and their interactions with boundary layer flows, our velocity spectra reveal unique turbulence structures that are modified by the thermodynamics of the fire fronts under various surface properties. Our results show good agreement with Clark et al. (1999) infrared camera imagery of convective dynamics during a crown fire. In both cases, convective motions during the fires had energy-containing eddies with spatial scales on the order of meters and time scales on the order of fractions of a second. There were also fire vortices on the scales of meters that continuously occurred at the fire front. The variations of low frequency or large scale turbulent energy and high frequency or fine-scale turbulent eddies suggest that the effects of the atmospheric boundary layer on fire behavior are quite large. Therefore, it is conceivable that turbulence certainly plays a fundamental role in the physics of fire spread.

3.1.4. Temperature spectra

Typical temperature-time variations in the plume above a fire front are characterized by a rapid rise to a maximum temperature after the fire's onset followed by a slow decrease in the temperature (Mercer and Weber, 2001; Clements, 2010). Since temperature perturbations from the mean during the FFP are much larger than velocity perturbations, all temperature spectra during the FFP (Fig. 7) show clear separations from the ambient spectra and lose the conventional shape of the surface layer temperature spectra shown by Kaimal et al. (1972), indicating that the temperature variations are independent from the surface layer temperature spectra within the fire environment. In addition, the characteristics of the −2/3 inertial subrange slope no longer appear at higher frequencies, and fluctuations of the spectral shape are more distinctive throughout the entire frequency range. This makes it difficult to identify the spectral peak frequency. It is suggested that during the FFP, fluctuations in both the horizontal and vertical components contribute to fluctuations in temperature because the horizontal velocity spectra show the dominant energy at the low frequency end and our vertical velocity spectra show most of the energy in the mid- to high-frequency range. It is also assumed that as the surface heating becomes strong and the convection-driven fire plume develops the influence of w on the temperature spectra increases and the influence of u decreases.

Bénech et al. (1986) presented temperature spectra observed at 25 m and 50 m above 1000 MW of artificially produced dry heat. Despite the fact that their standard deviations of the observed

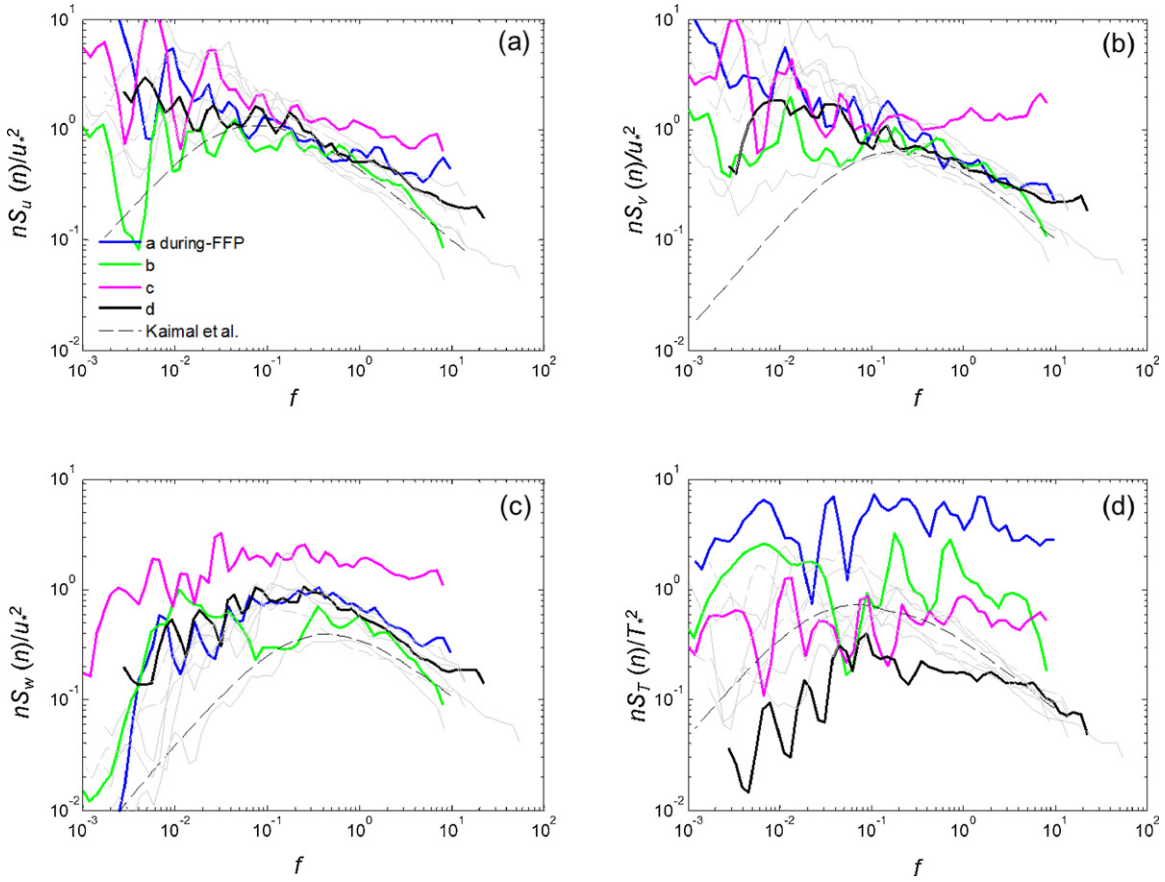

Fig. 9. Normalized spectra of velocity components and temperature observed during FFP for each experiment: (a) for u; (b) for v; (c) for w; and (d) for T as a function of the normalized frequency, $f = nz/U$. The dashed lines in the plots indicate the velocity and temperature spectra for neutral stability obtained by Kaimal et al. (1972). The pre- and post-FFP spectra shown in Fig. 8 are plotted with light gray color in the background.

temperatures were much higher within the plume than in the surrounding air even at the 50 m level, their temperature spectra show a distinct spectral peak on each curve with a roll-off of energy on both sides of the peak, regardless of measurement locations and heights above and around the heat source. Their temperature spectra exhibit a faster roll-off rate of −4/3 slope through the inertial subrange than the commonly observed −2/3 slope in the surface layer. They suggest that a local modification of production-dissipation balance resulted in the departure from the standard −2/3 slope at high frequencies and that the result is in good agreement with the observation made by Weill et al. (1976), who showed that the spectral slope of temperature fluctuation is likely to increase with the standard deviation of temperature. Their temperature measurements, however, were made using a platinum resistance thermometer that sampled at 3 Hz (Bénech et al., 1986) and thermistors digitized at 30 Hz after low-pass filtering (Weill et al., 1976). As far as the overall shape of temperature spectra are concerned, our results are in qualitative agreement with the results of Rotach (1995) who showed that within the urban canyon the distribution of temperature spectral densities is almost uniform (flat). Furthermore, a random distribution of temperature fluctuations and a small roll-off at the high-frequency end were also shown. Roth and Oke (1993) suggest that the deviation from the conventional spectral curve can be related to intermittent transfer processes coupling the air within the canyon with the flow above the canyon. Similarly, our flat temperature spectra were perhaps caused by intermittent convective heat influencing the major portion of the spectral energy as compared to the temperature fluctuations driven by surface layer characteristics.

A possible reason for the two different roll-off slopes that were observed is that ultra sonic temperatures were used in both our study and Rotach (1995) for the temperature spectral analysis as compared to the thermistors used in Bénech et al. (1986) and Weill et al. (1976). Our spectra were calculated from 10 Hz data while Rotach (1995) used 1 Hz data, and both showed similar spectral shapes. Thus, it seems that the difference in sampling rates does not contribute to the high frequency slope characteristics. Wieser et al. (2001) identified the increased roll-off slope at high frequency and pointed out that such attenuation was caused by the fact that the instrument used was not able to resolve the high-frequency fluctuations of the wind velocity. Wieser et al. (2001) added that such an effect should not occur in sonic anemometer data. Thus, it is possible that thermistors may not be able to sufficiently resolve high-frequency turbulent energy produced by wakes and small eddies. Katul et al. (1994) point out the limited resolution of thermocouples on the high wave-number end of the temperature spectrum and suggest that the sonic anemometer has better temporal resolution than thermocouples for temperature measurements. This may also be true for three component propeller anemometers when compared with ultrasonic anemometers, as it is shown by Yahaya and Frangi (2004) that dynamic characteristics of anemometers can result in different high frequency spectral behavior.

3.2. Normalized within the Monin–Obukhov similarity framework

A main advantage of normalizing spectra is to assess whether or not spectra collected under diverse conditions collapse into a

universal curve particularly in the inertial subrange. Fig. 8 presents the pre- and post-FFP spectra of the three velocity components and temperature for the four experiments. For clarity, the spectral densities of velocity have been multiplied by natural frequency n and normalized using ${u_*}^2$ following conventions established for Monin–Obukhov scaling. Similarly, the temperature spectra have been multiplied by natural frequency n and normalized using ${T_*}^2$. The normalized spectra are plotted against the non-dimensional frequency $f = nz/U$, where z is the measurement height, and U the horizontal mean wind speed. Without the influence of fire front passage, the velocity spectra are surprisingly well behaved in the sense that they follow the expected $-2/3$ slope and nearly collapsed into a narrow band in the inertial subrange, even the spectra measured within the canopy where Taylor's frozen eddy hypothesis is violated (e.g. σ_u/U is required to be less than 0.5 for measurements in time domain to be converted to space domain). The position of the velocity spectral peaks, which depends on the value of z/L presented in Table 3, seems to agree well with the generalized spectra observed over flat terrain as shown in Kaimal and Finnigan (1994). Although no systematic spectral behavior is expected when $z/L < 0$ (unstable atmospheric conditions) for horizontal velocity spectra, our horizontal velocity spectra fall into the spectral range shown in Kaimal and Finnigan (1994). The temperature spectra behaved well in the inertial subrange as they converged into the reference temperature spectra for neutral stability obtained by Kaimal et al. (1972).

All during-FFP velocity and temperature spectra are shown in Fig. 9. All velocity spectra except for the spectrum within the canopy collapsed into a reasonably narrow range in the inertial subrange, although they exhibit greater fluctuations than those before and after the FFP in Fig. 8, due to the perturbations induced by the fires. Nonetheless, the friction velocity, u_* works reasonably well as a scaling parameter for the velocity spectra during the FFP. In contrast, T_* may not be an appropriate scaling parameter as the normalized temperature spectra during the FFP do not show any systematic behaviors. This result is not surprising since the influence of the fire is so strong during the FFP that the temperature perturbations are independent of those in the surface layer. Consequently, the during-FFP spectra do not follow the reference curve obtained by Kaimal et al. (1972).

For the data considered, the inertial subrange of both the horizontal and the vertical spectra follow MOST, whereas we do not confirm a clear picture of their energy-containing regions in terms of the stability parameter. Although our results are based on limited data and include some inherent uncertainties, they do show a general agreement with the results of Kaimal et al. (1972) at the inertial subrange. The incomplete understanding of turbulence generation in and around wildland fires and their interaction with the surface layer invites further study to determine the applicability of MOST in fires.

4. Summary and conclusions

While field validation still remains as a major difficulty in developing realistic wildfire behavior models, this research describes qualitative aspects of turbulence behavior in the very small time and spatial scales involved in the convective processes that are associated with wildland fire front passage. The turbulence spectra in the atmospheric surface layer that was influenced by the fire's convective forcing were investigated by comparing those before, during and after the FFP. The spectral characteristics obtained from four unique field experiments were analyzed using existing simple numerical model results, laboratory experiments, and boundary layer concepts to identify some features that have not been adequately considered previously. Key findings from this study include the following:

- Increased horizontal mean winds and friction velocity are evident during the FFP. The biased variances also increased in both horizontal and vertical velocity components during the FFP.
- The vertical velocity and temperature variances presented in the nondimensional form as suggested by Monin–Obukhov similarity theory follow the local free convection behavior (Wyngaard et al., 1971) reasonably well under very unstable conditions ($z/L \ll -1$, during FFP), although the observations are better fitted with 1/2 power trend with $\phi_w = 1.3$ for the vertical velocity variance and with $-1/2$ power trend with $\phi_T = 1.4$ for temperature variance.
- Our results indicate a decreased degree of anisotropy in TKE during FFP.
- The horizontal velocity spectra during FFP show substantial increases at mid to high frequencies for all experiments due perhaps to fine-scale eddies that are shed from the fire, producing turbulent energy at a smaller scale than that produced by the ambient mean wind shear.
- Spectral behavior at mid to low frequency range may be affected by various environmental factors; increasing crossflow strength may inhibit the fire–atmosphere coupling. Consequently, spectral energy increases little at lower frequency. Our low intensity burn conducted under the canopy (EXP3) reveals pronounced energy increases at mid to high frequencies, whereas low frequency energy increased little due perhaps to the fact that the fire did not affect the mean winds above the canopy layer. A slash burn (EXP4) conducted under light ambient winds exhibited increased spectral energy at all frequencies, which may have been caused by strong fire–atmosphere coupling.
- Our vertical velocity spectra indicate substantial increases in nearly all frequencies. The strength of crossflow seems to affect the vertical velocity spectral behavior as well. The fire on the slope experiment (EXP2) that we conducted on a small hill produced a secondary w spectral peak at low frequency due probably to horizontal roll vortex formation.
- Our temperature spectra observed during FFP did not show the conventional spectral shape (i.e. Kaimal and Finnigan, 1994). The characteristic slope of the $-2/3$ inertial subrange was not observed at the high frequencies, resulting in "white noise" like spectra.
- The normalized velocity spectra observed during FFP collapsed fairly well onto a reference neutral curve of Kaimal et al. (1972) in the inertial subrange but did not converge as closely as the spectra observed before and after FFP. On the other hand, the normalized temperature spectra scatter randomly when scaled with T_* and did not show any systematic behaviors.

Our preliminary results show that fire can influence the energy of the flow and turbulence over a wide frequency range and therefore, emphasize the importance of the fire–atmosphere coupling in modeling physical and dynamical properties of wildland fires. Our experiments are limited to relatively low-intensity, controlled prescribed fires, where effects of mean flow strength, topography, and canopy layer on turbulence intensity are more significant than during larger and more intense wildfires. Further investigation of turbulence spectra during fire front passage is required to understand the applicability of the similarity law in wildland fires. Additionally, since many wildfires occur in complex mountainous terrain where localized wind systems already exist, those effects also need to be quantified more accurately for improved fire behavior prediction. Increased spatial density of turbulence measurements during larger experimental fires would also be beneficial to better understand the modification of fire–atmosphere interaction on large-scale surface layer flow.

Acknowledgements

The authors would like to first acknowledge the two anonymous reviewers for their suggestions and comments that greatly improved our analysis and manuscript. All experiments were supported by a Research Joint Venture Agreement with the USDA Forest Service – Northern Research Station (#07-JV-11242300-073). The sub-canopy experiments were supported by the Joint Fire Science Program (Award# 09-1-04-2). Dr. Tara Strand (Pacific Northwest Research Laboratory, USDA Forest Service) is acknowledged for her role as PI during the sub-canopy experiments. The authors thank the Cal Fire Santa Clara Unit (and in particular Battalion Chief Dave McLean) for conducting the prescribed burn in the valley location and for accommodating our research objectives. The Santa Clara County Department of Parks and Recreation is thanked for the special-use permit. The Contra Costa County Fire Department and other agencies involved in executing the planning and operations of the Wildfire 2010 training drill are acknowledged for accommodating our slope fire experiment. We thank Dennis Burns of the Pleasanton Fire Department for helping organize our research objectives into the burn plan. Travel support to participate in the IS4FIRES experiment is acknowledged from the Finnish Meteorological Institute, and in particular, Profs. David Schultz and M. Kumala. Janne Levula and Prof. Gerrit de Leeuw are thanked for help with the installation and the operation of our instrumentation at the Hyytiälä Forestry Field Station. The use of trade or firm names in this publication is for reader information and does not imply endorsement by the U.S. Department of Agriculture of any product or service.

References

Amiro, B.D., 1990. Drag coefficients and turbulence spectra within three boreal forest canopies. Boundary-Layer Meteorol. 52, 227–246.
Andreas, E.L., 1987. Spectral measurements in a disturbed boundary layer over snow. J. Atmos. Sci. 44, 1912–1939.
Anderson, D.H., Catchpole, E.A., de Mestre, N.J., Parkes, T., 1982. Modelling the spread of grass fires. J. Aust. Math. Soc. Ser. B 23, 451–466.
Albini, F.A., 1982. Response of free-burning fires to nonsteady wind. Combust. Sci. Technol. 29, 225–241.
Albini, F.A., 1983. The variability of wind-aided free-burning fires. Combust. Sci. Technol. 31, 303–311.
Al-Jiboori, M.H., Yumao, X., Yongfu, Q., 2001. Turbulence characteristics over complex terrain in west China. Boundary-Layer Meteorol. 101, 109–126.
Bénech, B., Noilhan, J., Druilhet, A., Brustet, J.M., Charpentier, C., 1986. Experimental study of an artificial thermal plume in the boundary layer. Part I. Flow characteristics near the heat source. J. Clim. Appl. Meteorol. 25, 418–437.
Cava, D., Giostra, U., Tagliazucca, M., 2001. Spectral maxima in a perturbed stable boundary layer. Boundary-Layer Meteorol. 100, 421–437.
Clark, T.L., Jenkins, M.A., Coen, J., Packham, D., 1996. A coupled atmosphere-fire model: convective feedback on fire-line dynamics. J. Appl. Meteorol. 35, 875–901.
Clark, T.L., Radke, L., Coen, J., Middleton, D., 1999. Analysis of small-scale convective dynamics in a crown fire using infrared video camera imagery. J. Appl. Meteorol. 38, 1401–1420.
Clements, C.B., 2010. Thermodynamic structure of a grass fire plume. Int. J. Wildland Fire 19, 895–902.
Clements, C.B., Zhong, S., Goodrick, S., Li, J., Bian, X., Potter, B.E., Heilman, W.E., Charney, J.J., Perna, R., Jang, M., Lee, D., Patel, M., Street, S., Aumann, G., 2007. Observing the dynamics of wildland grass fires: FireFlux – a field validation experiment. Bull. Am. Meteorol. Soc. 88 (9), 1369–1382.
Clements, C.B., Zhong, S., Bian, X., Heilman, W., Byun, D., 2008. First observations of turbulence generated by grass fire. J. Geophys. Res. 113, D22102, http://dx.doi.org/10.1029/2008JD010014.
Clements, C.B., Kukkonen, J., de Leeuw, G., Virkkula, A., Levula, J., Schultz, D.M., Kulmala, M., 2009. An overview of atmospheric measurements made during the IS4FIRES experiments at Hyytiälä, Finland. In: Eighth Symposium on Fire and Forest Meteorology, American Meteorological Society.
Coen, J., Mahalingam, S., Daily, J., 2004. Infrared imagery of crown-fire dynamics during FROSTFIRE. J. Appl. Meteorol. 43, 1241–1259.
Farge, M., 1992. Wavelet transforms and their applications to turbulence. Annu. Rev. Fluid Mech. 24, 395–457.
Finnigan, J.J., 2000. Turbulence in plant canopies. Annu. Rev. Fluid Mech. 32, 519–571.
Foken, T., 2006. 50 years of the Monin–Obukhov similarity theory. Boundary-Layer Meteorol. 119, 431–447.
Heilman, W.E., 1992. Atmospheric simulations of extreme surface heating episodes on simple hills. Int. J. Wildland Fire 2 (3), 99–114.
Heilman, W.E., Fast, J.D., 1992. Simulations of horizontal roll vortex development above lines of extreme surface heating. Int. J. Wildland Fire 2 (2), 55–68.
Hudgins, L., Friehe, C.A., Mayer, M.E., 1993. Wavelet transforms and atmospheric turbulence. Phys. Rev. Lett. 71 (20), 3279–3282.
Jenkins, M.A., Clark, T., Coen, J., 2001. Coupling atmospheric and fire models. In: Johnson, E.A., Miyanishi, K. (Eds.), Forest Fire: Behavior and Ecological Effects. Academic Press, pp. 257–302.
Kaimal, J.C., Wyngaard, J.C., Izumi, Y., Coté, O.R., 1972. Spectral characteristics of surface-layer turbulence. Quart. J. Roy. Meteorol. Soc. 98, 563–589.
Kaimal, J.C., Finnigan, J.J., 1994. Atmospheric Boundary Layer Flows. Oxford University Press, New York.
Katul, G.G., Parlange, M.B., Chu, C.R., 1994. Intermittency, local isotropy, and non-Gaussian statistics in atmospheric surface layer turbulence. Phys. Fluids 6 (7), 2480–2492.
Katul, G.G., Chu, C.R., 1998. A theoretical and experimental investigation of energy-containing scales in the dynamic sublayer of boundary-layer flows. Boundary-Layer Meteorol. 86, 279–312.
Katurji, M., Sturman, A., Zawar-Reza, P., 2011. An investigation into ridge-top turbulence characteristics during neutral and weakly stable conditions: velocity spectra and isotropy. Boundary-Layer Meteorol. 139, 143–160.
Kolmogorov, A.N., 1941. The local structure of turbulence in incompressible viscous fluid for very large Reynolds numbers. Dokl. Akad. Nauk SSSR 30, 299–303.
Kuznetsov, V.R., Praskovsky, A.A., Sabelnikov, V.A., 1992. Fine-scale turbulence structure of intermittent shear flows. J. Fluid Mech. 243, 595–622.
Larkin, N.K., O'Neill, S.M., Solomon, R., Raffuse, S., Strand, T., Sullivan, D.C., Krull, C., Rorig, M., Peterson, J.L., Ferguson, S.A., 2009. The BlueSky smoke modeling framework. Int. J. Wildland Fire 18, 906–920.
Lee, X., 2000. Air motion within and above forest vegetation in non-ideal conditions. Forest Ecol. Manage. 135, 3–18.
Lee, X., Black, T.A., 1993. Atmospheric turbulence within and above a Douglas-fir stand. Part 1. Statistical properties of the velocity field. Boundary-Layer Meteorol. 64, 149–174.
Lee, X., Massman, W., Law, B., 2004. Handbook of Micrometeorology. Kluwer Academic Publishers, Dordrecht, p. 250.
Liu, S., Liu, H., Xu, M., Leclerc, M.Y., Zhu, T., Jin, C., Hong, Z., Li, J., Liu, H., 2001. Turbulence spectra and dissipation rates above and within a forest canopy. Boundary-Layer Meteorol. 98, 83–102.
McNaughton, K.G., Laubach, J., 2000. Power spectra and cospectra for wind and scalars in a disturbed surface layer at the base of an advective inversion. Boundary-Layer Meteorol. 96, 143–185.
Mercer, G.N., Weber, R.O., 2001. Fire plumes. In: Johnson, E.A., Miyanishi, K. (Eds.), Forest Fire: Behavior and Ecological Effects. Academic Press, London, UK, pp. 225–355.
Morandini, F., Silvani, X., Rossi, L., Santoni, P., Simeoni, A., Balbi, J., Rossi, J.L., Marcelli, T., 2006. Fire spread experiment across Mediterranean shrub: influence of wind on flame front properties. Fire Safety J. 41, 229–235.
Nelson, M.A., Pardyjak, E.R., Klewicki, J.C., Brown, M.J., 2007. Properties of the wind field within the Oklahoma City Park Avenue street canyon. Part II. Spectra, co-spectra and quadrant analyses. J. Appl. Meteorol. Climatol. 46 (12), 2055–2073.
Panofsky, H.A., Larko, D., Lipschutz, R., Stone, G., Bradley, E.F., Bowen, A.J., Højstrup, J., 1982. Spectra of velocity components over complex terrain. Quart. J. Roy. Meteorol. Soc. 108, 215–230.
Quintiere, J.G., 1998. Principles of Fire Behavior. Delmar Publishers, Albany, NY, USA, 258 pp.
Rotach, M.W., 1995. Profiles of turbulence statistics in and above an urban street canyon. Atmos. Environ. 29 (13), 1473–1486.
Roth, M., Oke, T.R., 1993. Turbulent transfer relationships over suburban surface. Part I. Spectral characteristics. Quart. J. Roy. Meteorol. Soc. 119, 1071–1104.
Scire, J.G., Strimaitis, D.G., Yamartino, R.J., 2000. A User's Guide for the CALPUFF Dispersion Model (Version 5). Earth Tech Inc., Concord, MA.
Seto, D., Clements, C.B., 2011. Fire whirl evolution observed during a valley wind-sea breeze reversal. J. Combust. 2011, http://dx.doi.org/10.1155/2011/569475 (Article ID 569475, 12 pages).
Stull, R.B., 1988. An Introduction to Boundary Layer Meteorology. Kluwer Academic Publisher, Dordrecht, 666 pp.
Sun, R., Krueger, S.K., Jenkins, M.A., Zulauf, M.A., Charney, J.J., 2009. The importance of fire–atmosphere coupling and boundary-layer turbulence to wildfire spread. Int. J. Wildland Fire 18, 50–60.
Torrence, C., Compo, G.P., 1998. A practical guide to wavelet analysis. Bull. Am. Meteorol. Soc. 79 (1), 61–78.
Van Gorsel, E., Christen, A., Feigenwinter, C., Parlow, E., Vogt, R., 2003. Daytime turbulence statistics above a steep forested slope. Boundary-Layer Meteorol. 109, 311–329.
Weckman, E.J., Strong, A.B., 1996. Experimental investigation of the turbulence structure of medium-scale methanol pool fires. Combust. Flame 105, 245–266.
Weill, A., Aubry, M., Baudin, F., Heissat, J., 1976. A study of temperature fluctuations in the atmospheric boundary layer. Boundary-Layer Meteorol. 10, 337–346.
Wieser, A., Fiedler, F., Corsmeier, U., 2001. The influence of the sensor design on wind measurements with sonic anemometer systems. J. Atmos. Ocean. Technol. 18, 1585–1608.
Wilczak, J.M., Oncley, S.P., Stage, S.A., 2001. Sonic anemometer tilt correction algorithms. Boundary-Layer Meteorol. 99, 127–150.
Wyngaard, J.C., Coté, O.R., Izumi, Y., 1971. Local free convection, similarity, and the budgets of shear stress and heat flux. J. Atmos. Sci. 28, 1171–1182.

Yadav, A.K., Raman, S., Sharan, M., 1996. Surface layer turbulence spectra and dissipation rates during low winds in tropics. Boundary-Layer Meteorol. 79, 205–223.
Yahaya, S., Frangi, J.P., 2004. Cup anemometer response to the wind turbulence – measurement of the horizontal wind variance. Ann. Geophys. 22, 3363–3374.
Zhang, Y., Liu, H., Foken, T., Williams, Q.L., Liu, A., Mauder, M., Liebethal, C., 2010. Turbulence spectra and cospectra under the influence of large eddies in the Energy Balance EXperiment (EBEX). Boundary-Layer Meteorol. 136, 235–251.